Original

Herrmann-Geppert, I.; Bogdanoff, P.; Radnik, J.; Fengler, S.; Dittrich, T.; Fiechter, S.:

Surface aspects of solgel derived hematite films for the photoelectrochemical oxidation of water

Surface aspects of sol–gel derived hematite films for the photoelectrochemical oxidation of water†

Iris Herrmann-Geppert,*[a] Peter Bogdanoff,[b] Jörg Radnik,[c] Steffen Fengler,[b] Thomas Dittrich[d] and Sebastian Fiechter[b]

α-Fe$_2$O$_3$ (hematite) photoanodes for the oxygen evolution reaction (OER) were prepared by a cost-efficient sol–gel procedure. Due to low active photoelectrochemical properties observed, it is assumed that the sol–gel procedure leads to hematite films with defects and surface states on which generated charge carriers are recombined or immobilized in trap processes. Electrochemical activation was proven to diminish unfavourable surface groups to some extent. More efficiently, a plasma treatment improves significantly the photoelectrochemical properties of the OER. X-ray photoelectron spectroscopy (XPS) analysis reveals an oxygen enriched surface layer with new oxygen species which may be responsible for the improved electrochemical activity. Due to surface photovoltage an increased fraction of transferred charge carriers from these newly produced surface defects are identified.

Introduction

Analogous to photosynthesis, conversion of solar energy into chemical energy, *e.g.* by hydrocarbon or hydrogen formation, can be regarded as an option to store energy in large quantities. For this purpose, renewable energies such as wind and solar light can be used as energy sources to operate, for example, electrolysers contributing to a sustainable energy supply for mankind in the nearest future. But also a direct conversion is possible developing photocatalysts in photoelectrochemical electrolysers whose electrodes in contact with an aqueous electrolyte can directly split water into hydrogen and oxygen under illumination with sunlight. In such a system, an illuminated photoactive material generates excited charge carriers by the visible light absorption which can drive the redox reaction in the process of water splitting on the electrode surfaces in

contact with the aqueous electrolyte. However, the efficiency of such a device is limited by the kinetically hindered water oxidation reaction. To reduce present overvoltages at the electrode/electrolyte interface the photoactive electrode surface should be in addition catalytically active. This is necessary due to a four electron transfer mechanism at the water oxidizing photoanode where the activity is the rate limiting step in the process.

One promising material for the photo-induced oxygen evolution reaction (OER) is the mineral hematite (α-Fe$_2$O$_3$), which is cheap and abundant. Hematite has an ideal optical band gap of 2.2 eV and should in principle be able to oxidize water without any additional bias. It has an energetically spoken beneficially located valence band position as well as high corrosion stability.[1] However, the semiconductor also possesses unfavorable optoelectronic parameters such as a low diffusion length (L_D = 2–4 nm), a small absorption coefficient, a low electric conductivity and a low charge carrier mobility, so that the transport of photogenerated holes to the electrode surface to oxidize water molecules is generally limited. Consequently, recombination of the electron–hole pairs has to be overcome by increasing the diffusion length, enhancing the conductivity by doping and by the passivation of surface traps.[2–5] The implementation of nanotechnology in the process of electrode preparation to obtain an optimized architecture of the electrode can help us to surmount this problem.[6] Nevertheless the reaction mechanism of the water oxidation on hematite photoanodes is less understood. The group of Hamann concluded from a combination of electrochemical methods on atomic layer deposited (ALD) hematite

[a] *Helmholtz-Zentrum Geesthacht, Institute for Materials Research, Materials Technology (WTE), Max-Planck-Str. 1, 21502 Geesthacht and Helmut Schmidt University, University of the Federal Armed Forces Hamburg, Institute of Materials Engineering, Materials Science, Holstenhofweg 85, 22043 Hamburg, Germany. E-mail: iris.herrmann-geppert@hzg.de; Fax: +49 (0)4152 87-2636; Tel: +49 (0)4152 87-2562*

[b] *Helmholtz-Zentrum Berlin für Materialien und Energie, Institute for Solar Fuels, Hahn-Meitner-Platz 1, D-14109 Berlin, Germany*

[c] *Leibniz-Institut für Katalyse e. V. (LIKAT), Albert-Einstein-Str. 29a, 18059 Rostock, Germany*

[d] *Helmholtz-Zentrum Berlin für Materialien und Energie, Institute for Heterogeneous Materials, Hahn-Meitner-Platz 1, D-14109 Berlin, Germany*

† Electronic supplementary information (ESI) available. See DOI: 10.1039/c2cp42651j

This journal is © the Owner Societies 2013

Phys. Chem. Chem. Phys., 2013, **15**, 1389–1398 | **1389**

electrodes that the kinetic efficiency is limited to trapped photogenerated holes in surface states at moderate overpotentials. After a certain overpotential, holes can be transferred to proceed the following oxidation steps in the reaction.[7] Therefore the photogenerated holes need to be picked up in order to reduce the limiting trapping process and to reduce the overpotential. This was successfully demonstrated by the photoassisted electrodeposited cobalt phosphate catalyst (as suggested by Kanan and Nocera[8]) on these ALD deposited hematite films.[9] For further investigation of the charge carrier dynamics in hematite photoanodes transient absorption spectroscopy was applied in order to monitor the electron–hole recombination versus the applied potential.[10] From these studies it can be concluded that the surface composition and the resulting surface states of the hematite photoanodes play a crucial role in the catalytic efficiency in the photo-induced water oxidation reaction.

Recent progress in the development of the hematite photoanode has been achieved by the group of Grätzel.[11] They produced nanostructured iron oxide by chemical vapor deposition of hematite layers. Finally, the combination of the appropriate hematite nanostructure with a co-catalyst (IrO_2) leads to a highly efficient electrode material. Nanostructured iron oxide-based nanostructures can also be synthesized by wet chemical methods, which offer a cheaper and simpler method.

Although nanostructured hematite grown by a wet-chemical process reveals equal structural parameters compared with layer deposition from a gas phase reaction, a high photoactivity is only observed for the latter one (see ref. 12). This work is dedicated to further develop the sol–gel method to grow Fe_2O_3-based photoanodes of optimized layer thickness and to improve the oxide with respect to beneficial bulk and surface properties. Thereby post-treatments of the layers are applied which adjust the energetic properties of the bulk and the catalytic surface for the realization of an efficient photo-induced oxygen evolution reaction.

Experimental methods

Sol–gel preparation

The preparation of the films is described in detail in ref. 13. Briefly summarized, nanocrystalline hematite films were obtained by a sol–gel procedure adapted to the Pecchini method.[14] 0.01 mol $Fe(NO_3)_3$ was added to a solution containing 0.05 mol citric acid (99.5% from Aldrich) and 0.1 mol ethylene glycol (99.5% from Merck) at 80 °C under reflux. The resulting yellow solution was then heated at 120 °C for two hours.

After cooling down, the brown sol–gel (resin consistency) was diluted in ethylene glycol in a 4 : 3 ratio and constantly stirred for thirty minutes. The resin-type sol–gel was deposited on fluorine-doped tin-oxide (FTO) glasses by dip coating (v = 2.27 cm s^{-1}). Afterwards the films were calcinated in a split-hinge furnace in an air atmosphere at 500 °C for 2 hours (heating rate: 1 K min^{-1}). The dip coating and calcination procedure was repeated two times in order to gain a sufficient layer thickness with respect to the absorption length.

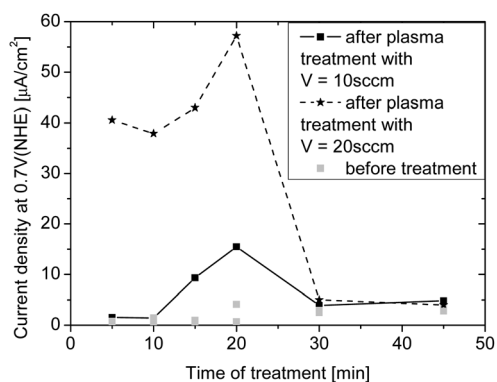### Post-treatment of the hematite film: anodic polarisation

Electrochemical treatment of the hematite films was performed in a Differential Electrochemical Mass Spectroscopy set-up (DEMS, see below). Firstly, cyclic voltammograms (CVs) of the hematite film were measured at 2 mV s^{-1} under dark conditions and under illumination (100 mW cm^{-2}) in N_2-purged neutral media (0.1 M KH_2PO_4 buffer solution). Afterwards a constant potential of 2 V(NHE) was applied for 20 min. Mass signals m/q = 32 (O_2) and 44 (CO_2) were detected during the experiment. Subsequently, after electrochemical treatment CV of the treated hematite film was measured again.

Post-treatment of the hematite film: oxygen plasma treatment

Plasma treatment was performed using a plasma etcher from Diener electronics at Optotransmitter Umweltschutz Technologie e.V. company (OUT e.V., Berlin). The films were placed in the reaction chamber with their conducting side facing upwards. The free FTO part of the slides was covered by glass during the treatment in order to maintain a good back contact. The chamber was evacuated until an oxygen partial pressure of 0.2 mbar was reached. Optimisation of the plasma treatment was performed in pre-experiments by varying the gas flow and the treatment time. In Fig. 1 the photocurrent of plasma treated samples is plotted versus the treatment time. The photocurrent increases with increasing treatment time and increased oxygen gas flow, firstly. After a certain maximum the photocurrent declines again. It was suggested that this negative effect is evoked by abrasion of the hematite layer. Optimised parameters were chosen for the plasma treatment of the hematite films. In the presented experiment an oxygen gas flow of 20 sccm was established. The sample was treated for 20 min in the plasma.

Electrochemical characterisation

Electrochemical measurements (except for the experiments with DEMS) were performed in a three-electrode compartment controlled by an EG&G potentiostat (Type 273A). Thereby, the films were contacted as working electrodes by a gold wire via

Fig. 1 Variation of plasma parameters. Grey symbols present the photocurrent of the hematite film before the plasma treatment. Photocurrents of the plasma treated samples with 20 sccm are plotted versus their treatment time with the black stars. Photocurrents of the plasma treated samples with 10 sccm are plotted versus their treatment time with the black squares.

the FTO glass outside of the electrolyte. A platinum wire was used as a counter electrode and an Hg/HgO reference electrode was utilized in 1 M KOH (+0.1 V vs. NHE). Iron oxide electrodes were cycled at 20 mV s^{-1} under anodic conditions to 1 V(NHE) in 1 M KOH until the cyclic voltammogram (CV) curve showed steady state characteristics. CVs under dark conditions and illumination were performed. The sample was illuminated through a small orifice (0.3117 cm^2) using a 400 mW cm^{-2} tungsten halogen lamp from Xenophot. For the potentiostatic measurements at 0.7 V(NHE) the film was illuminated with intermittent pulses for 30 s.

Differential electrochemical mass spectroscopy

The details of the differential electrochemical mass spectroscopy (DEMS) are given in ref. 15 and 16. The inlet system between the electrochemical cell and the differential pumped vacuum system of the mass spectrometer (Balzers; QMI 420, QME 125, QMA 125 with 90° off axis SEM) consists of a porous hydrophobic membrane. The working electrode is closely attached to this membrane so that a remaining thin film of the electrolyte between the membrane and the electrode enables electrochemical experiments. Oxygen, which is formed in an electrochemical experiment at the Fe_2O_3-working electrode surface, diffuses to some extent into the mass spectrometer where it is detected simultaneously with the electrochemical data. Except for the anodic polarisation (see above), experiments were carried out in N_2-purged 1 M KOH at a scan rate of 2 mV s^{-1}. For the photo-induced reaction the films were illuminated using a tungsten halogen lamp from Xenophot (100 mW cm^{-2}). As a reference a mercury oxide electrode (+100 mV) and as a counter electrode a Pt-wire were used. All data given in this paper are related to the standard hydrogen potential (NHE).

UV-Vis spectroscopy

Optical analysis was performed using a Lab950 UV-Vis spectrometer (from Perkin Elmer) equipped with a 150 mm integrating sphere. Reflected and transmitted light from the hematite sample is detected using an InGaAs detector.

Transmission electron microscopy

The hematite films were embedded in an epoxy-type matrix for the cross-sectional TEM analysis. Sliced samples were investigated by employing a Philips CM12 transmission microscope.

X-ray photoelectron spectroscopy (XPS)

XPS measurements have been performed using an ESCALAB220 iXL spectrometer (Fisons). The spectrometer works with monochromated Al-Kα-radiation (1486.6 eV). The analysis was carried out by "Universal Spectrum Processing and Analysis Program" (Unifit 2011).

Raman spectroscopy

Raman spectra were measured using a LabRam spectrometer (Jobin Yvon) at room temperature. For excitation the 632 nm line of an He/Ne laser was used. Samples were pressed as KBr

pellets. By means of an optical microscope (Olympus BX), the sample has been placed in the focus of the beam. In order to separate Raman and Rayleigh scattering, a notch filter and a monochromator were utilized. Finally, a CCD camera detected the Raman bands.

Surface photovoltage measurements

SPV measurements were performed in the fixed capacitor arrangement at a modulation frequency of 8 Hz. The measurements were carried out at 0.02 mbar. A halogen lamp with a quartz prism monochromator was used for illumination. SPV signals were detected with a high impedance buffer (Elektronik Manufaktur Mahlsdorf, RC time constant larger than 1 s) and a double phase lock-in amplifier. The phase of the lock-in amplifier was adjusted with a Si photodiode whose response time was much faster than the measurement period. The SPV amplitude resulted from the square root of the sum of the squared in-phase and by 90° phase-shifted SPV signals. The tangent of the so-called phase angle was the ratio between the by 90° phase-shifted and in-phase SPV signals. A phase angle of 0° corresponds to very fast charge separation and relaxation in comparison to the modulation period while the electrons are separated preferentially towards the internal surface. A change of the phase angle (values <90°) corresponds to a change of the retardation of charge separation and relaxation.

Results and discussion

Films from the sol–gel process reveal a dark red color which is typical for hematite (13). By cross-sectional TEM analysis (see Fig. 2), a film thickness of about 400 nm was evaluated. In detail, UV-Vis measurement revealed a pronounced absorption edge in the red region ranging from 500 to 600 nm (see Fig. 3). Interestingly, transmission and reflectance curves differ slightly versus the wavelength. In the cross-sectional TEM analysis
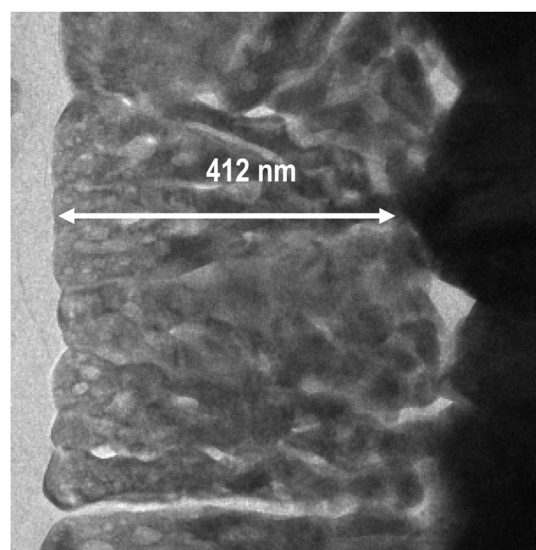
Fig. 2 Cross-sectional TEM analysis of hematite film grown by the sol–gel process.
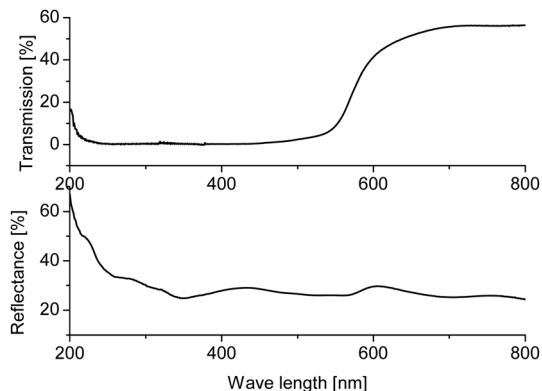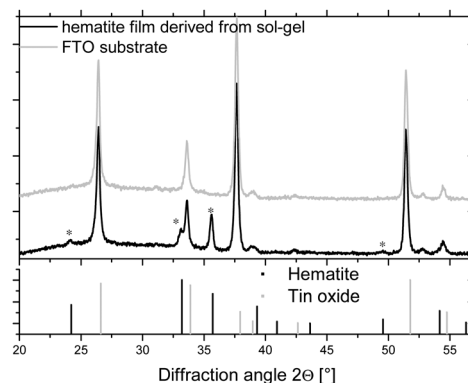
Fig. 3 UV-Vis measurement of the hematite film grown by the sol–gel process: (top) transmission and (bottom) reflectance measurements.
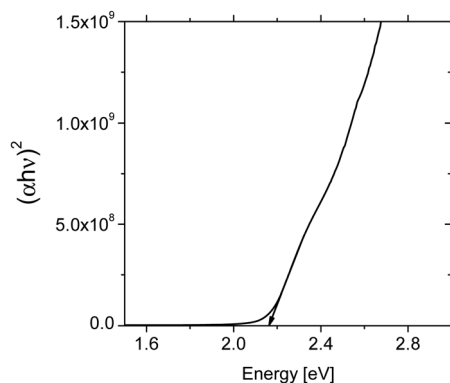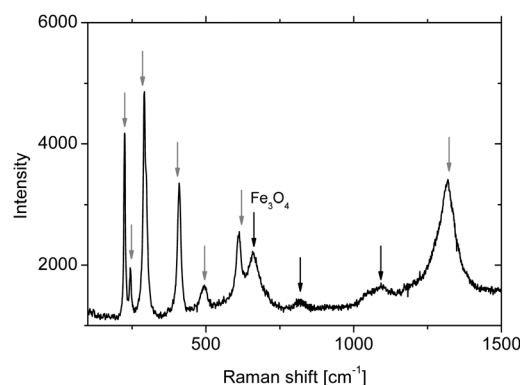

**Fig. 4** Determined Tauc plot of the hematite film grown by the sol–gel process.

Fig. 5 XRD diffractogram of the hematite film grown by the sol–gel process and of the pristine FTO substrate with the corresponding XRD lines for hematite and tin oxide. The stars present the detected lines for hematite in the films.

Fig. 6 Raman spectrum of the hematite film grown by the sol–gel process (Raman main bands of hematite (referred in ref. 18) are marked with grey arrows and discussed additional bands are marked with black arrows).

(see Fig. 2) it is observed that the upper layer consists of smaller particles than the particles of the lower layer. This morphology is caused by repeating the procedure of dip coating and heat treatment. Due to their small size these particles can act as scattering centres for the blue and UV light leading to an increased reflectance. Furthermore, interferences of the scattered light provoke differences in the reflectance and transmission data. The Tauc plot of the direct transition was calculated as suggested in ref. 17 (see Fig. 4). From the extrapolation a direct band gap at 2.17 eV was determined for the investigated films. From this it can be concluded that charge carriers are generated by the visible light absorption.

XRD analysis of these films revealed small XRD lines of the hematite besides the more pronounced reflexes of the FTO substrate (see Fig. 5). Thus, it is verified that crystalline hematite is formed in the sol–gel process.[13] Besides XRD analysis Raman spectroscopy was also performed for the structural characterization (see Fig. 6). According to the literature,[18] the typical Raman bands of hematite were found. The sole exception is the Raman band at 658 cm^{-1} which indicates the presence of magnetite (Fe_3O_4) in the sample. In the latter Raman analysis of the plasma treated and untreated hematite films, the broad peak at 658 cm^{-1} is deconvoluted in two weak peaks at 610, 634 and in one pronounced at 657 cm^{-1}. The low peak intensity in contrast to the pronounced hematite Raman

bands implies that there is only a low concentration of magnetite in the film. So far it could not be clarified whether this side-product influences the photoelectrochemical properties of the films. In the work of Singh et al., it is noted that magnetite is more electrically conductive than hematite.[19] But at this point it is not clarified whether the magnetite particles exist separately besides the hematite ones or are layered on the hematite particles. That is why it is difficult to predict the effect on the photoactivity of the hematite films due to the presence of magnetite. Raman bands of magnetite were also found in the literature, however, in the Raman analysis of the highly active hematite films obtained from plasma spraying and gas phase reaction due to the reduction of hematite at high temperatures.[20,21] Two weaker bands are detected at 818 and in the range between 1040 and 1090 cm^{-1}. This Raman band range is typical for C–C and C–H vibrations from hydrocarbons.[22] That is why the origin of this weaker Raman bands might be speculated as the latter discussed residual carbon-based species from the decomposed polymer network (see above).

Photoelectrochemical measurements were performed in alkaline media (see Fig. 7). The CV curve under dark conditions reveals an anodic current starting at ca. 0.6 V(NHE). This indicates a moderate
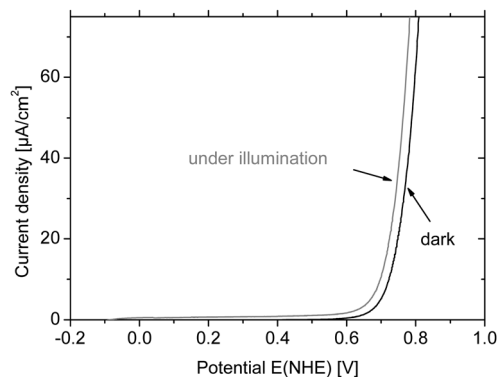
Fig. 7 Cyclic voltammetry (CV) curves of a hematite film grown by the sol–gel process under illumination (grey, tungsten halogen lamp 400 mW cm^{-2}) and under dark conditions (black) (scan rate: 20 mV s^{-1}) in 1 M KOH.

overpotential towards the thermodynamic equilibrium potential at 0.4 V(NHE, pH = 14). Under illumination the photo-induced current is shifted to negative potentials only by 50 mV at 2 μA cm^{-2}. This low difference between the dark and photocurrent indicates problems in establishing photovoltage in the hematite photo-catalyst. Because the process of visible light absorption is confirmed by UV-Vis measurements (as mentioned above), the generated charge carriers obviously are not available for the water oxidation reaction. This could be due to an inefficient charge separation, recombination processes or capturing of holes in deep traps. This suggestion is confirmed also in time-dependent potentiostatic measurements (see Fig. 8). When the hematite film is illuminated, an instant high photocurrent is observed which relaxes very fast to a steady state level. In the literature[23] this needle-type photocurrent behavior is explained as follows: the instant high current is due to the flux of photo-generated charge carriers towards the surface. Due to a hindered electrochemical reaction, they accumulate at the surface and recombine to some extent. The subsequent fast decay towards the steady state shows the saturation of this accumulation layer. The remaining photocurrent results from a competition between recombination processes and the slow electrochemical kinetics of the OER. Furthermore it is noted that
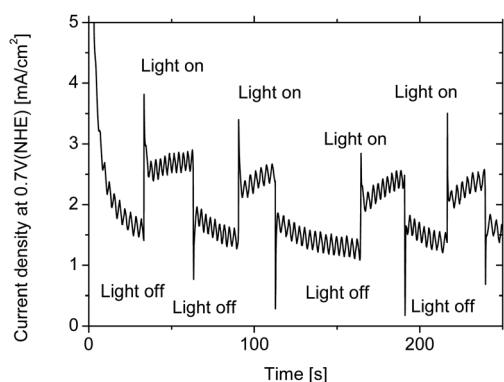
Fig. 8 Potentiostatic measurement of a hematite film grown by the sol–gel process at 0.7 V(NHE) in 1 M KOH with intermittent light pulses (400 mW cm^{-2} tungsten halogen lamp, pulse length 30 s).
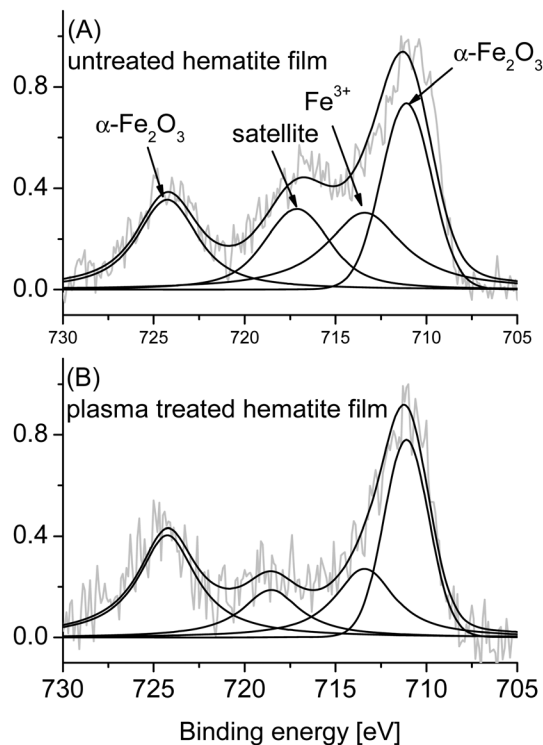
Fig. 9 Fe2p spectra of (A) an untreated hematite film grown by the sol–gel process and (B) a plasma treated hematite film.

this photocurrent additionally shows a slow increase which origi-nates from a heating effect during illumination.

The hematite surface was analyzed by XPS measurements. It is noticed that the films reveal a high carbon concentration (C/Fe = 214). In the C1s spectrum three peaks are fitted in the spectrum (not shown). Concerning the literature,[24] these peaks can be attributed to hydrocarbons (285 eV), C–OH (287 eV) and carboxyl and/or carbonyl surface groups (289 eV). These carbon compounds might originate from decomposition products of the organic based polymer network of the sol–gel and might influence the water oxidation reaction. As discussed above, these undesired surface groups evoke surface states at which the charge carriers are trapped and can recombine.

The Fe2p spectrum (see Fig. 9A) shows a broad peak at around 711 eV, which can be attributed to a mixed Fe(3+)–Fe(2+) valence state of Fe2p3/2.[25] The maximum of this peak is shifted to higher binding energy, so a higher amount of Fe(3+) can be expected. Nevertheless reported XPS studies of hematite in the literature observed and simulated similar curve course of the Fe2p core-level spectra. The peak at around 725 eV is related to Fe2p1/2 and the peak at 719 eV is the corres-ponding satellite.

It is assumed that the carbon-based polymer presents a reduction environment during the hematite formation so that a lower oxidation state of iron is obtained. It is not clarified how possible side products (e.g. Fe_3O_4) influence the charge carrier recombination and, endlessly, the reactivity on the surface. In correlation with the observed photoelectrochemical properties on the untreated hematite films it is suggested that generated

charge carriers cannot contribute to the electrochemical oxidation of water. The detected surface adsorbents generate surface states at which the photogenerated holes can recombine with electrons or can be immobilized in trap processes.
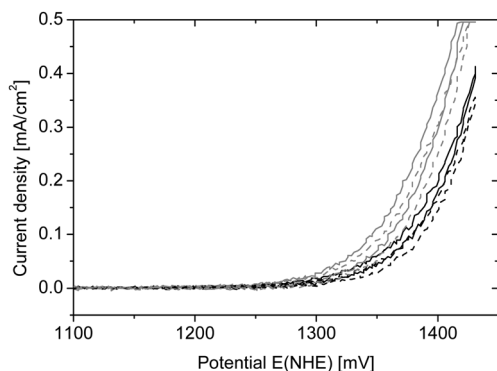
Anodic polarisation

Due to these unfavorable surface properties for the photooxidation of water surface treatments were applied in order to remove the undesired surface groups. In the first approach an electrochemical activation of the hematite films was applied in neutral media under an anodic potential (2 V(NHE)). For this electrochemical treatment the differential electrochemical mass spectroscopy (DEMS) technique was chosen in order to track the gaseous products during the activation. The DEMS set-up is described in detail in the Experimental methods section.
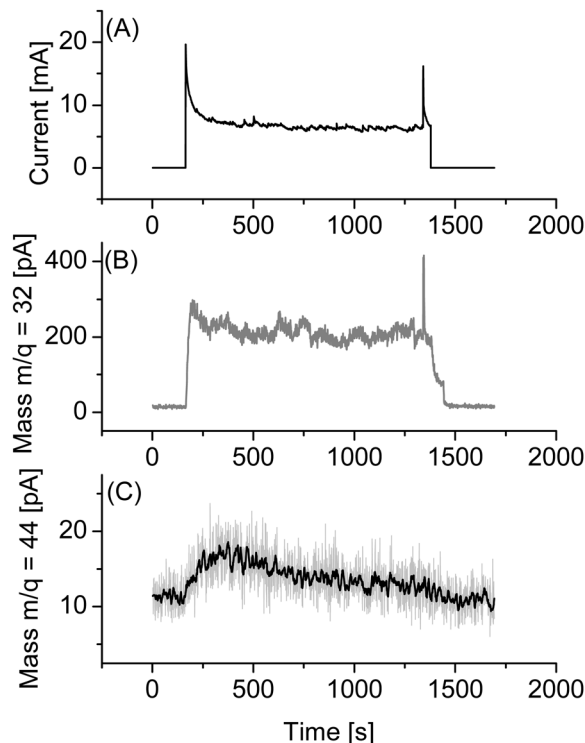
Before anodic polarization the film was electrochemically characterized. In Fig. 10 the CV curve is presented. The anodic current starts at ca. 1.3 V(NHE) under dark conditions. Accordingly, the photo-induced current is only shifted by 10 mV in this experiment. Obviously, similar low photoelectrochemical properties are detected in neutral and alkaline media.

In Fig. 11 the potentiostatic curve of the anodic polarization combined with the detected mass signals $m/q = 32$ for oxygen and 44 for carbon dioxide are presented. Under anodic conditions the oxygen signal steeply increases under illumination which indicates the oxygen evolution reaction. During the experimental time the oxygen evolution is nearly constant. Furthermore the mass signal 44 for CO_2 is observed which is due to oxidation of the surface carbon. Finally the signal declines to zero which indicates the complete oxidation of carbon.

After this anodic polarization the electrochemical properties of the hematite film were tested again. In Fig. 10 the CV curve after treatment is also presented. The dark and photocurrent reveals a slightly increased slope but the onset potential of the photo-induced water oxidation remained constant. Although the carbon-based surface groups were removed, the catalytic surface properties were only slightly improved. Apparently, the
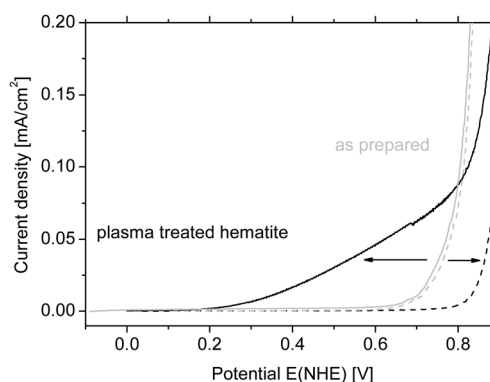

Fig. 11 Differential electrochemical mass spectroscopy (DEMS) measurement during the anodic polarisation of a hematite film at 2 V(NHE) in 0.1 M KH_2PO_4 buffer solution, illuminated with 100 mW cm^{-2}. (A) Potentiostatic curve at 2 V(NHE), (B) mass signal of $m/q = 32$ (for oxygen) and (C) mass signal of $m/q = 44$ (for carbon dioxide).

carbon-based species do not play a crucial role in the photoelectrochemical properties of the hematite films.

Oxygen plasma treatment

In our recent publications, ref. 13 and 26, we demonstrated that the photoelectrochemical properties of the hematite films, discussed here, can be drastically improved by a treatment in oxygen plasma. In ref. 26 the electrochemical results are discussed in detail. In the following a brief summary is given. In Fig. 12, the CV curves before and after the plasma treatment

Fig. 10 Cyclic voltammetry (CV) curves of the hematite films before (grey) and after the anodic polarisation (black) at 2 mV s^{-1} in 0.1 M KH_2PO_4 buffer solution (measured in the DEMS set-up) (dotted lines – under dark conditions, solid lines – under illumination (100 mW cm^{-2})).


Fig. 12 Cyclic voltammetry (CV) curves of the hematite films before (grey) and after oxygen plasma treatment (black).
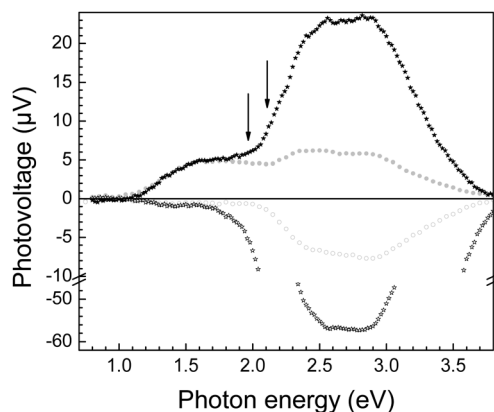
Fig. 13 Surface photovoltage measurements of films before (grey) and after oxygen plasma treatment (black) (filled squares and stars – in-phase, empty squares and stars – phase-shifted by 90°).

Fig. 14 Potentiostatic measurement of a hematite film before (grey) and after oxygen plasma treatment (black) at 0.7 V(NHE) in 1 M KOH with intermittent light pulses (400 mW cm^{-2} tungsten halogen lamp) for 30 s.

are presented. In contrast to the untreated material, the dark current of the plasma treated sample is shifted significantly to more positive potentials. It was suggested that electrochemical active surface groups energetically located below the redox potential of the water oxidation reaction are diminished and therefore the Fermi level has to be shifted to more positive potentials in order to generate holes for the water oxidation. The onset of the photocurrent is shifted from *ca.* 400 mV to *ca.* 200 mV(NHE) by the internal generated photovoltage of the semiconductor. This remarkable improvement of the photo-voltage was also seen in surface photovoltage measurements, as discussed in detail in ref. 26. In Fig. 13 the measured SPV curves before and after the plasma treatment are presented. Mainly, more band to band transitions were provided for the charge carrier separation after the plasma treatment. Because the ionised gas from the oxygen plasma also attacks the metallic support pad for the sample, heating also occurs during the treatment. That is why it was assumed that the surface layer can be re-crystallized due to the heating during the plasma treatment. Thereby defects, contributing to the recombination, are reduced. Furthermore an increased part of the surface photovoltage was detected which originates from a new inter-band transfer. It was suggested that a new surface state is generated by the plasma treatment so that an enhanced charge carrier separation is provided. This results in drastically increased photocurrents as it is shown in potentiostatic measurements (see Fig. 14). The now less pronounced initial current peak points to the fact that recombination processes seem to be diminished. Due to the plasma treatment the photocurrent at 0.7 V(NHE) is increased from *ca.* 5 µA cm^{-2} to 58 µA cm^{-2}.

Apparently, the attack of oxygen plasma radicals leads to a reorganization of the surface. Due to the increased photocur-rent it is suggested that recombination processes are reduced and active catalytic sites are generated on the surface. In the following surface analysis of the plasma treated hematite film these points are closely investigated. In XPS analysis it was found that the carbon concentration remains nearly constant.
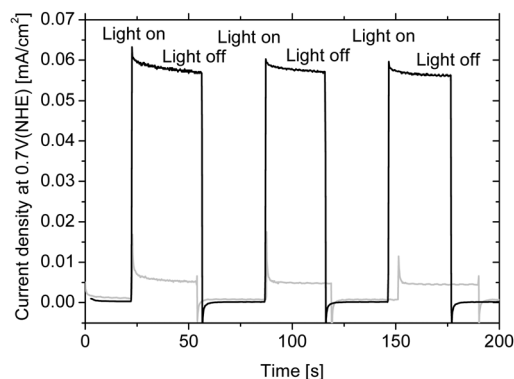
Although carbon-based species are oxidized in the plasma etching process, the re-adsorption of carbon-based compounds due to the exposure to air might lead to this surface decoration. It is noted again that the carbon-based species adsorbed on the surface do not play a crucial role in the photoelectrochemical properties of the hematite film. Nevertheless the oxygen concentration is increased from O/Fe = 451 to O/Fe = 539. Comparing O1s spectra of the untreated and plasma treated films the spectra indicate changes of the oxygen surface chemistry of the films (see Fig. 15). The peaks with higher binding energy are more pronounced in the O1s spectrum of the plasma treated film. Interestingly, the fitting of the broad signal leads to a new peak at
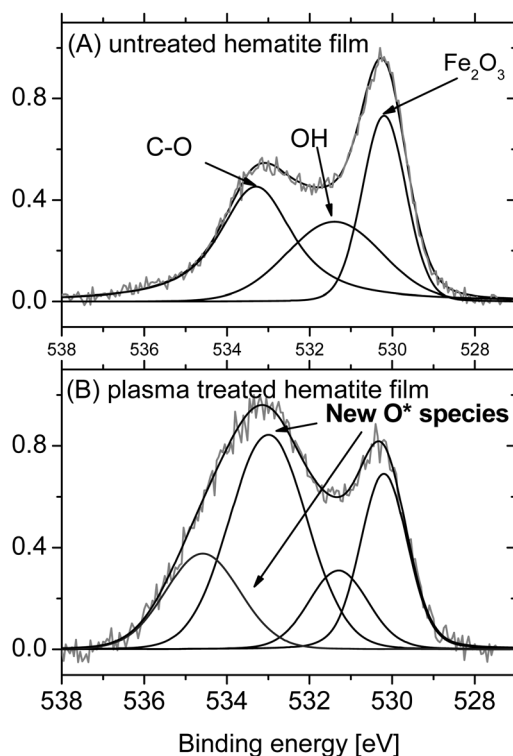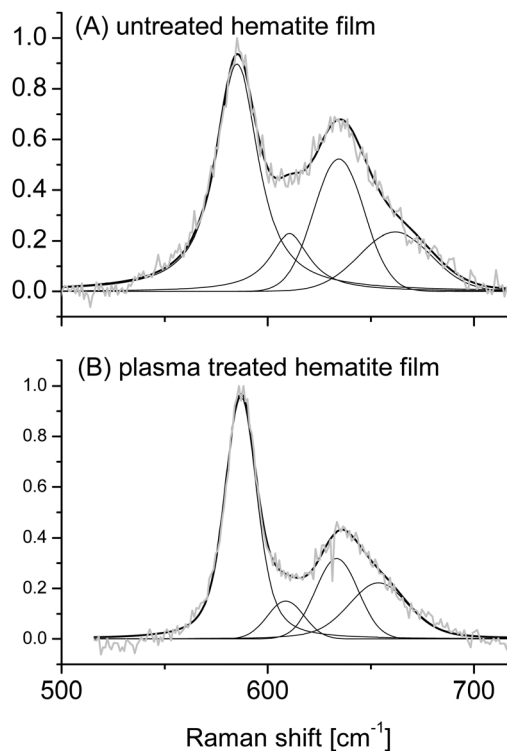

Fig. 15 O1s spectra of (A) an untreated hematite film and (B) a plasma treated hematite film.
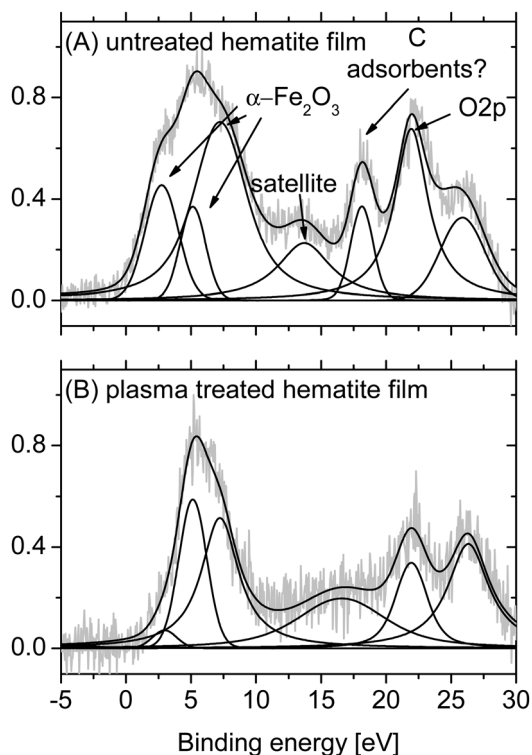
Fig. 16 Valence band (VB) region of (A) an untreated hematite film and (B) a plasma treated hematite film.

Fig. 17 Deconvolution of the Raman spectra in the range between 500 and 700 cm^{-1} of (A) an untreated hematite film and (B) a plasma treated hematite film.

534.6 eV in the O1s spectrum. From the high binding energy it is concluded that oxygen species with strong binding are present in the surface layer. From the literature these species could be attributed to a large amount of oxyhydroxides.[27,28] In further advanced experiments the chemical composition of this oxygen-based surface structure will be investigated. As the activity increases with the appearance of these peaks, we assume that these new oxygen species are responsible for the improved photocurrent.

Nevertheless, the Fe2p spectra of hematite films, discussed here, are only slightly changed due to the plasma treatment (see Fig. 9). From analysis of the peak ratio it can be inferred that the area of the Fe^{3+} peak is slightly lowered related to the other peaks. The changes of the hematite become more apparent in the comparison between the valence band regions of the plasma treated and untreated hematite film (see Fig. 16). Three states belong to the valence bands (VBs) of hematite were found at 2.8, 5.2 and 7.3 eV.[25] Furthermore a peak at 18.2 eV was found in the VB spectrum of the untreated sample which might be correlated to adsorbed carbon-based species. While valence bands of the untreated hematite film show broad signals, the ratio of the hematite VB peaks of the plasma treated sample is changed related to each other, for example the peak at 5.2 eV is most pronounced after the plasma treatment, while the dominant peak is 7.3 eV in the untreated sample. Furthermore, the hematite peaks become sharp. From this comparative analysis it is speculated that states in the band gap were restricted to a few defined ones due to the plasma treatment.

This is in agreement with the surface photovoltage measurements which proved the enhanced band to band transition.

For further study of the effect of the plasma treatment, Raman spectra before and after the plasma treatment are discussed (see Fig. 17). The distribution of the hematite peak intensities does not change significantly (not shown here). But in the detailed view of the Raman spectra in the range between 500 and 700 cm^{-1} the Raman band at 657 cm^{-1} is decreased in relation to the hematite band at 585 cm^{-1}. This band is attributed to magnetite. Furthermore it is noted that the Raman band at 585 cm^{-1} for hematite reveals a more narrow distribution which indicates a more homogeneous chemical composition. Apparently, magnetite is transferred to hematite due to the oxygen radical attack in the plasma treatment process. Because the appearance of magnetite and its extent of the effect on the photoactivity is not clarified at this point, it can only be speculated that the transfer from magnetite to hematite might improve the photoelectrochemical properties.

From the XPS surface analysis it is concluded that the composition of the surface layer is changed due to an oxygen enrichment. The surface photovoltage measurement of the plasma treated hematite film shows an increased established photovoltage in the hematite film. This indicates an enhanced charge carrier separation towards the electrochemical interface due to the plasma treatment. It seems to be likely that the formed junction from the bulk to the oxygen enriched surface layer generates an electric field in the film. This leads to a better transport of the photogenerated charge carriers directed
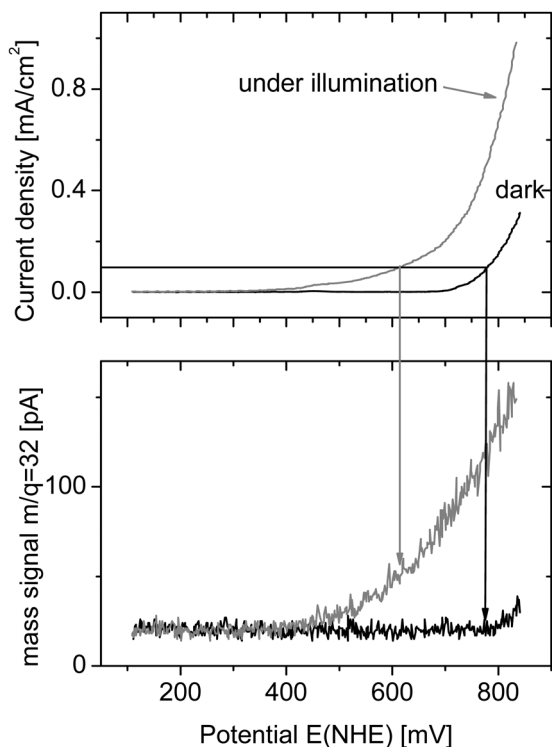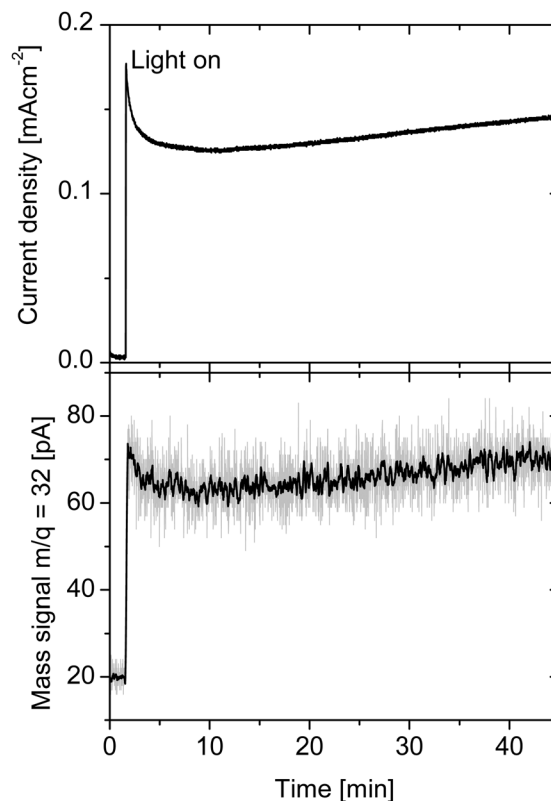
Fig. 18 Differential electrochemical mass spectroscopy (DEMS) measurement of a plasma treated hematite film measured in 1 M KOH at a scan rate of 2 mV s⁻¹ in the dark (black) and under illumination (100 mW cm⁻² of a tungsten halogen lamp) monitoring the mass signal m/q = 32 detecting oxygen evolution.

Fig. 19 Potentiostatic measurement of a plasma treated hematite film measured at 0.64 V(NHE) in 1 M KOH in the DEMS-set up under illumination (100 mW cm⁻² light intensity of a tungsten halogen lamp) monitoring the mass signal m/q = 32 detecting oxygen evolution.

towards the electrode/electrolyte interface. This thesis is supported by the SPV measurements.

Finally, DEMS measurements of the post-treated hematite are discussed. In Fig. 18 the photocurrent and dark currents of the post-treated hematite film accompanied with the detected mass signal m/q = 32 for oxygen measured in the DEMS set-up are presented. Looking at the threshold of oxygen release it is found that the oxygen evolution is initiated at 400 mV(NHE) on hematite electrodes under illumination. Under dark conditions the onset of the oxygen evolution is detectable at values >800 mV(NHE).

Interesting phenomena related to oxygen formation were observed comparing similar anodic current densities, e.g. at 0.1 mA cm⁻², under illumination and in the dark. Related to the detected mass signals at a certain current density it was noted that the oxygen production at a current density e.g. 0.1 mA cm⁻² was found to be smaller under dark conditions than under illumination. Probably corrosion processes are partially involved in the dark water oxidation reaction, which are induced at high positive potentials.

Finally, a potentiostatic measurement at 0.64 V(NHE) for 40 min (see Fig. 19) demonstrated stable oxygen production in this time frame. Interestingly, the photocurrent slightly increases during the experiment time. In the literature,[12] new charge carrier transfer behaviour was found when the hematite film was electrochemically oxidised. This new surface structure, subsequently formed under an applied potential, might enable

an energetically more favorable carrier transfer of the photo-generated holes.

Conclusions

Charge-carrier recombination and trapping processes were hypothesized as reasons for low photoelectrochemical activity towards the water oxidation reaction for hematite photoanodes prepared by a cost-efficient sol–gel procedure. It was suggested that unfavourable surface states, in terms of carbon-based surface groups, caused by the production process are present. Electrochemical treatment by anodic polarisation was probed in which surface carbon was oxidised. Nevertheless, a significant improvement of the photo-induced water oxidation reaction was absent. From this it was concluded that carbon-based surface groups or adsorbents do not play a crucial role in the loss of excited charge carriers.

Oxygen plasma treatment leads successively to a significantly increased photocurrent and internal generated photovoltage. From structural investigation, it was found that an oxygen enriched surface is formed during plasma treatment. In Raman spectra it is also observed that the side product magnetite (Fe_3O_4) is diminished which is transferred to hematite. Furthermore new oxygen species are detected by XPS analysis which are correlated to the improved catalytic surface

This journal is © the Owner Societies 2013

Phys. Chem. Chem. Phys., 2013, **15**, 1389–1398 | **1397**

properties. The new surface states are formed close to the valence band which are believed to be responsible for the enhanced charge transfer kinetics across the electrode/electrolyte interface in the water oxidation reaction.

Acknowledgements

Notes and references

1 R. van de Krol and M. Grätzel, *Photoelectrochemical Hydrogen Production*, Springer US, New York, 2012, p. 121.
2 F. Le Formal, N. Tétreault, M. Cornuz, T. Moehl, M. Grätzel and K. Sivula, *Chem. Sci.*, 2011, **2**, 737.
3 D. A. Wheeler, G. Wang, Y. Ling, Y. Li and J. Z. Zhang, *Energy Environ. Sci.*, 2012, **5**, 6682.
4 T. W. Hamann, *Dalton Trans.*, 2012, **41**, 7830.
5 M. T. Meyer, C. Du and D. Wamg, *J. Am. Chem. Soc.*, 2012, **134**, 12406.
6 Y. Lin, G. Yuan, S. Sheehan, S. Zhou and D. Wang, *Energy Environ. Sci.*, 2011, **4**, 4862.
7 B. Klahr, S. Gimenez, F. Fabregat-Santiago, J. Bisquert and T. W. Hamann, *Energy Environ. Sci.*, 2012, **5**, 7626.
8 M. Kanan and D. Nocera, *Science*, 2008, **321**, 1072.
9 B. Klahr, S. Gimenez, F. Fabregat-Santiago, J. Bisquert and T. W. Hamann, *J. Am. Chem. Soc.*, 2012, **134**, 16693.
10 S. R. Pendlebury, A. J. Cowan, M. Barroso, K. Sivula, J. Ye, M. Grätzel, D. R. Klug, J. Tang and J. R. Durrant, *Energy Environ. Sci.*, 2012, **5**, 6304.
11 K. Sivula, F. Formal and M. Grätzel, *ChemSusChem*, 2011, **4**, 432.
12 D. K. Bora, A. Braun, S. Erat, A. K. Ariffin, R. Löhnert, K. Sivula, J. Töpfer, M. Grätzel, R. Manzke, T. Graule and E. C. Constable, *J. Phys. Chem. C*, 2011, **115**, 5619.
13 I. Herrmann-Geppert, P. Bogdanoff, L. Hepperle and S. Fiechter, *ECS Trans.*, 2012, **41**(33), 201.
14 M. P. Pecchini, *US Patent*, No. 3.330.697, 1967.
15 P. Bogdanoff and N. Alonso-Vante, *J. Electroanal. Chem.*, 1994, **379**, 415–421.
16 P. Bogdanoff and N. Alonso-Vante, *Ber. Bunsen-Ges. Phys. Chem.*, 1993, **97**, 940–942.
17 J. Tauc, R. Grigorovic and A. Vanc, *Phys. Status Solidi*, 1966, **15**, 627.
18 D. L. A. de Faria, S. Venancio Silva and M. T. de Oliveira, *J. Raman Spectrosc.*, 1997, **28**, 873.
19 A. P. Singh, S. Kumari, R. Shrivastav, S. Dass and V. R. Satssangi, *J. Phys. D: Appl. Phys.*, 2009, **42**, 085303.
20 C. J. Sartoretti, B. D. Alexander, R. Solarska, I. A. Rutkowska and J. Augustynski, *J. Phys. Chem. B*, 2005, **109**, 13685.
21 A. Duret and M. Grätzel, *J. Phys. Chem. B*, 2005, **109**, 17184.
22 M. R. Fenske, W. G. Braun, R. V. Wiegand, D. Quiggle, R. H. McCormick and D. H. Rank, *Anal. Chem.*, 1947, **19**, 700.
23 C. Y. Cummings, F. Marten, L. M. Peter, A. A. Tahir and K. G. U. Wijayantha, *Chem. Commun.*, 2012, **48**, 2027.
24 K. Kinoshita, *Carbon: Electrochemical and Physicochemical Properties*, John Wiley & Sons, 1988, p. 116.
25 T. Fujii, F. M. F. Groot and G. A. Sawatzky, *Phys. Rev. B: Condens. Matter Mater. Phys.*, 1999, **59**(49), 3195.
26 I. Herrmann-Geppert, P. Bogdanoff, S. Fengler, T. Dittrich and S. Fiechter, *ECS Trans.*, 2012, submitted.
27 T. Hanawa, S. Hiromoto, A. Yamamoto, D. Kuroda and K. Asami, *Mater. Trans.*, 2002, **43**, 3088.
28 S. Yamamoto, T. Kendelewicz, J. T. Newberg, G. Keteler, D. E. Starr, E. R. Mysak, K. J. Andersson, H. Ogasawara, H. Bluhn, M. Salmeron, G. E. Brown and A. Nilsson, SLAC-PUB-13827, 2009.